AIMS Energy, 10(6): 1165–1189.
DOI: 10.3934/energy.2022055
Received: 05 September 2022
Revised: 15 November 2022
Accepted: 16 November 2022
Published: 22 November 2022

http://www.aimspress.com/journal/energy

Research article

Integration of wind and tidal turbines using spar buoy floating foundations

Navid Majdi Nasab [1,*], Jeff Kilby [1] and Leila Bakhtiaryfard [2]

[1] Electrical and Electronic Engineering Department, School of Engineering, Computing and Mathematical Sciences Auckland University of Technology, 1010 Auckland, New Zealand
[2] Technology Research Department, R&D Centre, Fusheng Industrial Co., Ltd, 24158 Taipei, Taiwan (R.O.C.)

* **Correspondence:** Email: navid.nasab@aut.ac.nz; Tel: +642102975454.

Abstract: Floating platforms are complex structures used in deep water and high wind speeds. However, a methodology should be defined to have a stable offshore structure and not fail dynamically in severe environmental conditions. This paper aims to provide a method for estimating failure load or ultimate load on the anchors of floating systems in integrating wind and tidal turbines in New Zealand. Using either wind or tidal turbines in areas with harsh water currents is not cost-effective. Also, tidal energy, as a predictable source of energy, can be an alternative for wind energy when cut-in speed is not enough to generate wind power. The most expensive component after the turbine is the foundation. Using the same foundation for wind and tidal turbines may reduce the cost of electricity. Different environment scenarios as load cases have been set up to test the proposed system's performance, capacity and efficiency. Available tidal records from the national institute of Water and Atmospheric Research (NIWA) have been used to find the region suitable for offshore energy generation and to conduct simulation model runs. Based on the scenarios, Terawhiti in Cook Strait with 110 m water height was found as the optimized site. It can be seen that the proposed floating hybrid system is stable in the presence of severe environmental conditions of wind and wave loadings in Cook Strait and gives a procedure for sizing suction caisson anchors.

Keywords: wind; moment load; floating; deflection; tilt

1. Introduction

1.1. Rational of hybriding marine technologies

With the increasing electricity demand and global warming attributed to the combustion of fossil fuels, exploitation of offshore energy sources in the form of wind, sea currents, and waves has attracted the global pursuit of renewable energy [1].

While a life cycle analysis (LCA) of offshore wind generation against onshore shows a 48% improvement in the project's sustainability, the cost of electricity using offshore wind is still high [2,3]. The generation of tidal energy is also expensive. This obstacle makes investment in tidal turbines difficult as harsh water currents decrease the design life, and at deep-sea levels, the foundation design is complicated [4]. Using the same foundation for wind and tidal turbines can reduce the cost of electricity by increasing power generation enabled by two different sources of energy [5]. However, if a support structure is not correctly designed for offshore conditions, failure will be disastrous, and the structure will be costly to replace. For this reason, foundations are an essential design consideration. Aspects to be considered while choosing and designing the foundation for a particular site include weather conditions, seabed geology, vessels and equipment required to install, and protecting the environment in accordance with local regulations.

Deployed on floating bodies or along with cables, offshore energy harvesters can convert wave, solar, tidal, ocean current, and other renewable energy sources to stable electrical energy [6]. Hybrid them with wind electricity generation would reduce the currently significant operations & maintenance (O&M) of a wind turbine (WT) which is around 10–25% of the total cost of the electricity, and a lower transmission cost [7,8].

By bringing together two marine renewable technologies with considerable synergies, the combined harnessing of offshore energies presents an excellent potential for development. This is corroborated by some recent European Union (EU) funded projects: MARINA, ORECCA, TROPOS, MERMAID and H2OCEAN [9]. MARINA classifies combined wave-wind systems according to the technology, water depth (shallow, transition, or deep water), or location relative to the shoreline (shoreline, nearshore, offshore). ORECCA analyses the offshore renewable energies (ORE) combined resources in Europe. Looking particularly at the combined wave-wind resource in Europe, this can be divided into three main sea basins: the Mediterranean Sea, North and Baltic Seas, and the Atlantic Ocean. TROPOS is aimed at developing a floating multi-purpose platform system for deep water [9]. The MERMAID project seeks to develop concepts for the next generation of offshore activities for multi-use of ocean space. It proposes new design concepts for combining offshore activities, like energy extraction, aquaculture, and platform-related transport at various ocean areas [10]. H2OCEAN is developing a wind-wave power open-sea platform equipped for hydrogen generation with support for multiple energy users [11].

1.2. Literature review of floating offshore systems

Floating systems are the best solution for mass production in deep water sites where bottom fixed turbines are uneconomical and can be installed easier in offshore environments. Depending on how floating offshore turbines achieve their stability, they can be categorized into three main concepts, spar buoy, Tension Leg Platform (TLP), and semi-submersibles. A spar buoy foundation enhanced stability

by adding ballast water. It is based on the concepts of spar buoy and Tension Leg Platform (TLP), which maintains its stability through a mooring system and buoyancy [12,13]. The mooring system has six degrees of freedom inhabiting motion while connecting to the seabed, making it possible to operate under different water depths [14,15]. This flexibility makes its market broader and more economical for investment in any range of water height [15]. In recent decades, there has been a great tendency to move from standing-driven foundations in the seabed to floating moored foundations. This is illustrated by shifts from fixed foundations working less than 60 m of water (e.g., Vindey Denmark 2017) to floating moored foundations in 120 m of water (e.g., Hywind Scotland 2018) and even to 1000 m of water (e.g., 2021 call for proposals from Bureau of Ocean Energy Management (BOEM) in California, USA) [16]. Currently, the key companies of spar buoys are Hywind/Statoil (Norway), Toda (Japan), Sway (Norway), NauticrAft (Australia) and SeaTwirl (Sweden) [17].

In recent years, many researchers have worked in the application of floating offshore domain in oil and gas platforms. Musial et al. [18] have observed that individual mooring and anchor costs are significant for single-turbine systems compared to a shared system. Fontana et al. [19] investigated the hydrodynamic performance and loading analysis of shared anchors for various FOWT configurations and found that shared anchors must be structurally strong enough to handle loading from unexpected directions. Anchors with a directional preference in their holding position and capacity are generally not suited for multi-line moorings, but they can be adapted by extra structural outfitting for handling mooring loads in various directions [20]. The type of floater is also found to have a significant influence on the anchor forces. Balakrishnan et al. [21] analyzed and compared the anchor forces on a semi-submersible floater system and a spar-type floater system and found that the anchor forces on the latter were less. This is because spar-type platforms have less surface area interacting with waves compared to that of a semi-submersible. Goldschmidt and Muskulus [22] investigated the performance of coupled-mooring systems involving 1, 5 and 10 floaters in various configurations. Semi-submersible floaters were arranged in a row and triangular and rectangular configurations separately, and the system dynamics were studied. It was found that mooring system cost reductions up to 60% and total system cost reductions up to 8% were achievable using shared moorings. However, it was noted that the displacements of the floaters were higher when the number of floaters in the system increased, which would be a problem for large wind farms. Further investigation is required to improve the behavior of floaters in larger wind farms.

2. Concept description

In contrast to grounded foundations, aerodynamic and hydrodynamic loads create considerable motion for floating ones [15]. So, it is essential to define a straightforward methodology to estimate the loads on the anchor to establish a feasibility analysis [13]. The paper aims to provide a simplified approach for finding the maximum allowable loads necessary for a foundation which can support the selected wind and tidal turbines with spar buoy foundation. An example of offshore wind and tidal turbines supported on a floating spar is then considered based on the environmental data from NIWA. Finally, a simplified anchor sizing procedure is presented, demonstrating conservative upper bound estimates for the required suction caisson for Cook Strait. What is novel described in this paper is that it defines a method of foundation design of integrated wind and tidal structures in deep water using spar buoy floating in terms of structural modelling. The methodology used in this research for hybrid foundation design is an improved method for current method which was used before for foundation

design of wind turbine.

The design will be carried out by developing spreadsheets relevant to different aspects of foundation design based on standard IEC 61400, IEA Wind TCP Task 37-May 2019, DNV 2014 and IEC 2019 [23–26].

A single long column extends far below the water to dampen movement using water and sand as the ballast shown in Figure 1. It is loosely anchored to the sea floor. It is also loosely moored to the sea floor [17]. The total ballast is approximately 8,000 tons, split between a solid part and water. The percentage split and type of ballast material are subject to further design optimization. The ballast water will typically be dosed with lye, and NaOH, giving a pH value above 10.5 [27].

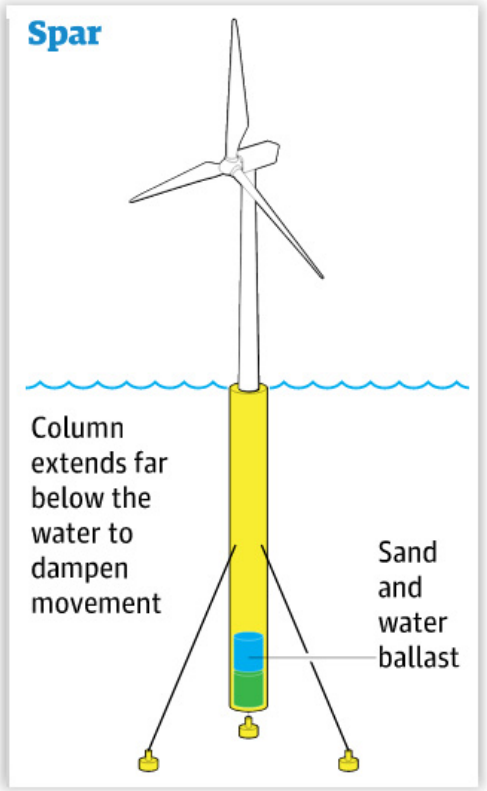

Figure 1. The mechanism of enhancing the stability of the spar by adding water ballast [17].

The base case is secured to the seabed using suction anchors. The suction anchors are likely to have a maximum diameter of 7 m, corresponding to an estimated footprint of 40 m^2 per anchor. Suction anchors are designed such that 1 m of sand erosion/scouring is acceptable. The base case is that there is there is no need for rock dump around anchors to prevent scour. However, due to the likely presence of mobile sediments in the area, scour protection around the anchors may be required to some extent (e.g., rock dumping, mattresses). The footprint of such scour protection is expected to extend no more than 15 m out from the anchor perimeter [27].

The schematic structure of turbines installed with a floating foundation is shown in Figure 2.

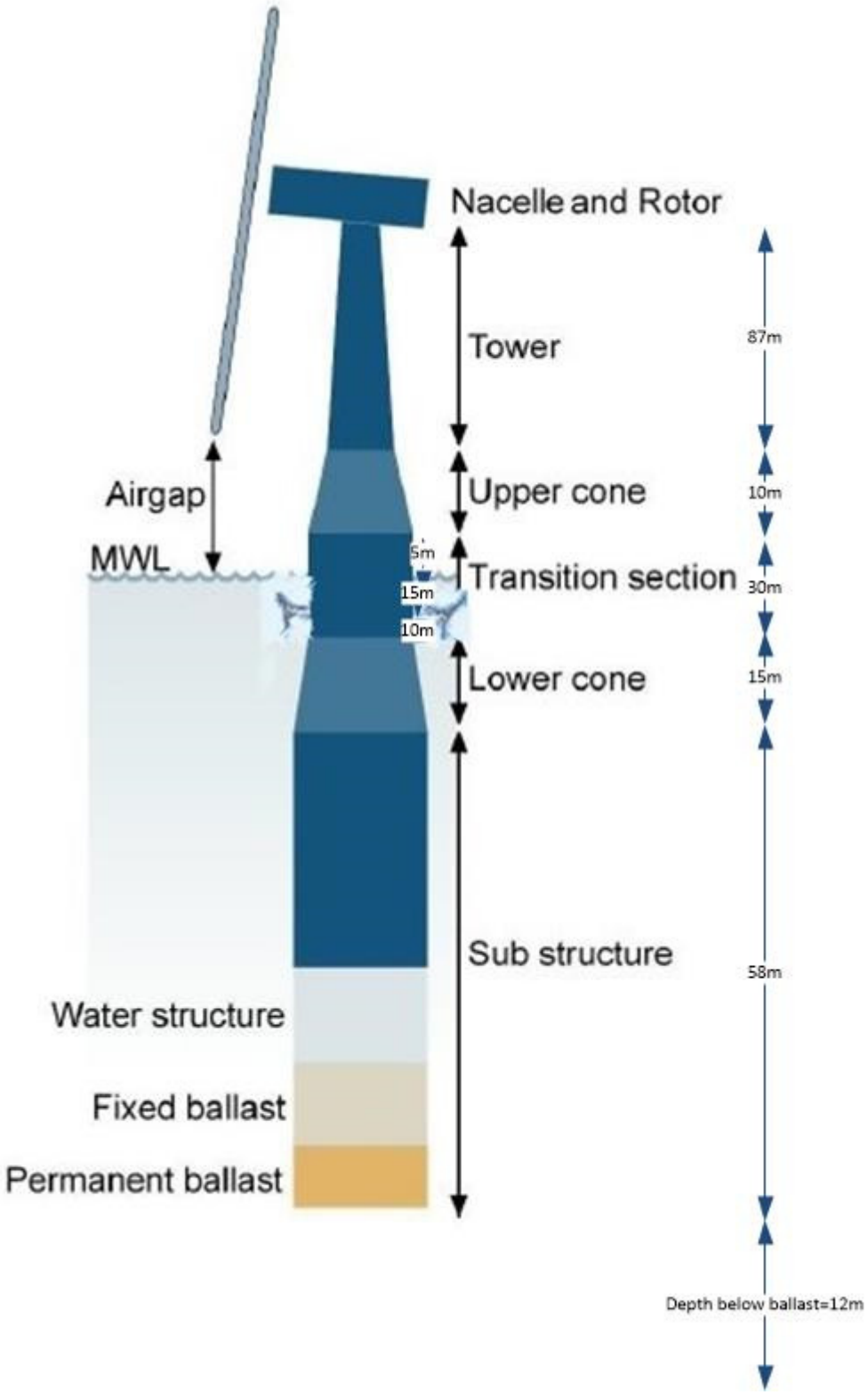

Figure 2. General view of the support structure.

Table 1 summarizes the features of the proposed foundation considering the total weight of wind and tidal turbines used for the hybrid system is approximately equal to the Statoil turbine. Key design parameters will receive further discussion in section 5 [28].

Table 1. General information on the spar mooring parameters.

Parameter	Symbol	Value	Unit
Spar diameter	D_S	14	m
Spar draft (depth below sea level)	B	93	m
Length of upper/lower cone	L_C	10	m
Diameter of the lower cone (upper section)	-	6	m
Diameter of the upper cone (lower section)	-	6	m
Diameter of the upper cone (upper section)	-	5	m
Mass of ballast	m_B	8000	tons
Mass of spar buoy	m_S	1000	tons
Mooring radius	r_m	700	m
Diameter of mooring chains		130	mm
Unit weight of mooring chains	μ_C	300	kg/m
Mass of the mooring cables	m_S	350	tons

3. Environmental parameters for design

Severe environmental conditions where the wind speed and the significant wave height have a large value are more common in deep water seas [14]. Therefore, tidal current modelling conducted by MetOcean Solutions Limited (MSL) was used for site optimization [29]. The resolution of this model in the NZ-wide grid is 0.06° (5.6 × 6.6 km). MetOcean used The Princeton Ocean Model (POM) model with a high-resolution domain over Cook Strait (0.002°; 170 × 230 m) as the best area for offshore supply, as shown in Figure 3 [30]. POM was used in a vertically integrated two-dimensional mode with boundaries provided by the global TPX0 solution [31].

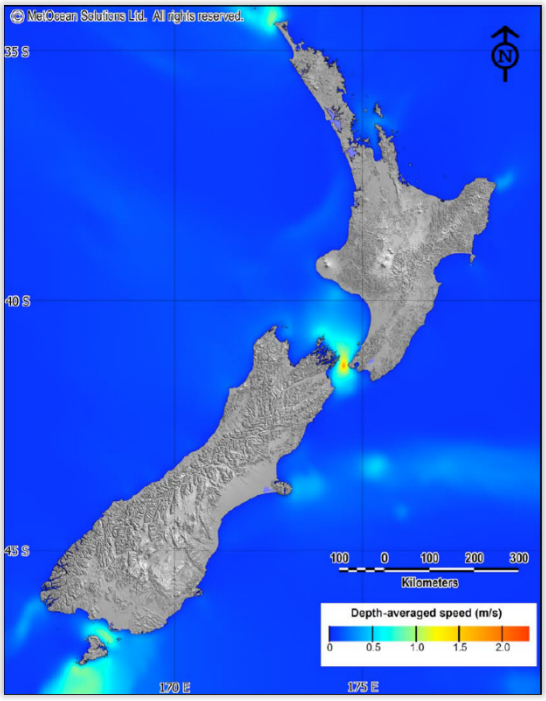

Figure 3. National depth-averaged tidal current speeds for mean spring flows (in m/second) [30].

The main geographical parameters of the optimized site in Cook Strait are shown in Table 2.

Table 2. Tide data for Terawhiti [32,33].

Location	Latitude (deg)	Longitude (deg)	Annual water velocity (m/s)	Depth of water (m)	Annual wind velocity (m/s)
Terawhiti	−41.3138°S	174.5898°E	1.32	110	7.10

The most important data from NIWA's [34] analysis is summarized in Table 3.

Table 3. Wave data for Terawhiti.

Parameter	Symbol	Value	Unit
Significant wave height with a 50-year return period [35]	Hs	15	m
Peak wave period	Ts	13.73	s
Maximum wave height (50 years)	Hm	27.62	m
Maximum wave peak period	Tm	18.63	s
Maximum water depth (50-year high water level)	S	30	m
Water density	ρ_w	1030	kg/m^3

Equivalent wind data will be sourced from the meteorological recording site closest to the Terawhiti taken from NASA. This data will be presented in Table 4 and Figure 4. These data are essential to estimate the wind stresses transmitted through the turbine's support structure to its foundation.

Table 4. The geological and geotechnical wind data of Terawhiti [23,36–38].

Parameter	Symbol	Value	Unit
Shape parameter-Weibull distribution [37]	s	1.98	[-]
Scale parameter-Weibull distribution [37]	K	7.99	m/s
Reference turbulence intensity [23]	I	16	%
Turbulence integral length scale [36]	L_K	340.2	m
Annual wind speed [33]	u_{ave}	7.10	m/s
Air density [36]	ρa	1.225	kg/m^3

Naturally, the wind's speed constantly varies. In order to be able to predict a wind turbine 's production it is necessary to know exactly how often the wind blows how strongly. Normally, the wind is measured with an anemometer and the mean wind speed is recorded every 10 minutes. This data can be sorted into wind speed classes of 1 m/s each. The energy contained in the wind at a certain site may then be expressed by this frequency distribution. The Weibull distribution is often a good approximation for the wind speed distribution. The Weibull two-parameter distribution function often describes wind speed variability. It is considered a standard approach for evaluating local wind load probabilities because it has been found to fit a wide collection of wind data [39]. The Weibull shape and scale parameters are denoted by s and K, respectively. It is dimensionless and indicates how peak the site under consideration is, while K has a unit of wind speed (m/s), and it shows how windy the site is [40].

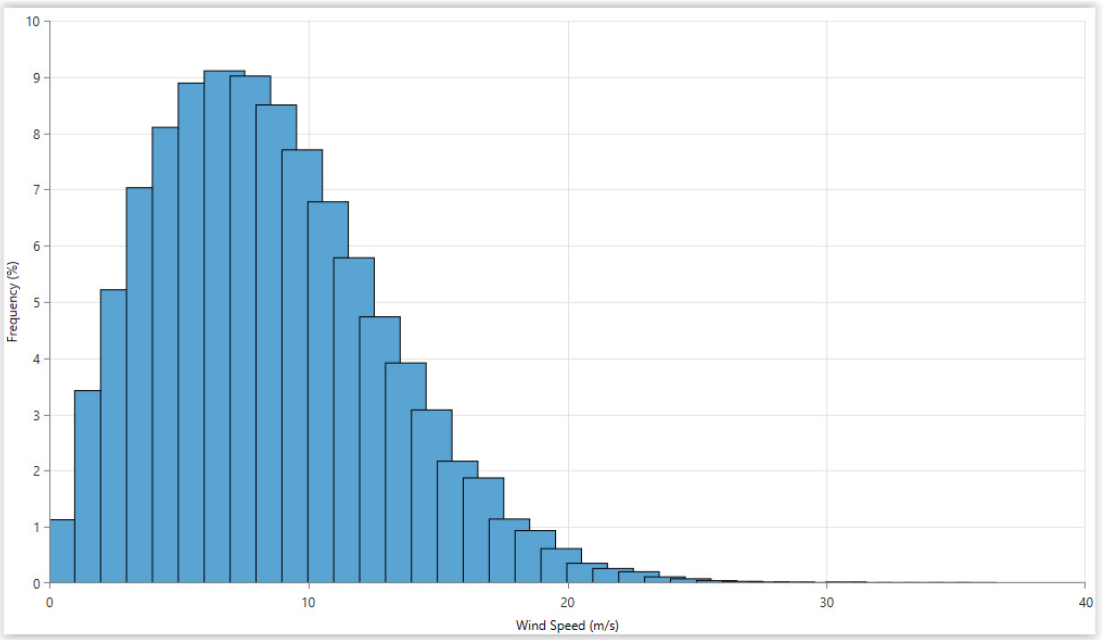

Figure 4. Wind speed histogram for Terawhiti [33].

To calculate the Weibull parameters, the frequency percentage of Terawhiti results by Homer is used in the Weibull calculator [37], which results in s = 1.98 and K = 7.99 m/s.

The turbulence intensity varies with mean wind speed, which for Terawhiti is 7.10 m/s, and quantifies how much the wind varies typically within 10 minutes [36]. The reference turbulence intensity value (16%) may be obtained from the IEC 61400 standard [23].

Based on the DNV code, for height above sea level (z) less than 60 metres, Lk is 5.67z, and for z above 60 meters, Lk is 340.2 meters [36]. As the height above sea level is 87m, the turbulence integral length scale is 340.2 m in this case.

4. Methods

The steps given in Figure 5 are used to evaluate the feasibility of an offshore hybrid structure in Cook Strait.

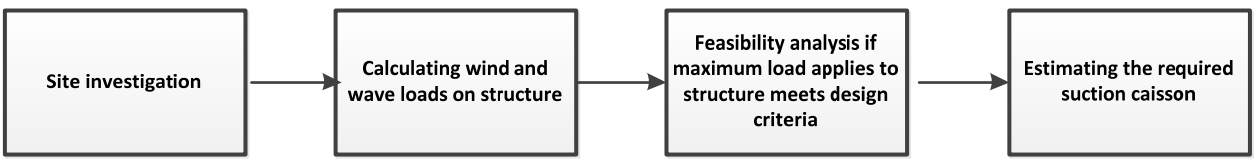

Figure 5. Design process of floating wind and tidal structure.

The design criteria which will be checked for the possibility of a floating design are presented in Table 5.

Table 5. Main criteria for foundation design [36].

Parameter	Limit
The maximum stress (σ_m)-yield strength (f_{yk})	$\sigma_m < f_{yk}$
Deflection (ρ_0)	$\rho_0 < 0.2\ m$
Tilt (θ_0)	$\theta_0 < 0.5\ °$
The structural natural frequency(f_0) -frequency of rotation of the rotor ($f_{1P,\ max}$)	$f_0 > 1.1 f_{1P,\ max} = 0.24$ Hz
Pile wall thickness (t_P)	$t_P \geq 6.35 + \frac{D_P}{100}$

Design criteria specific to the selected turbines are presented in Tables 6 and 7.

Table 6. General information of wind turbine, Siemens SWT-3.6-107 offshore 3.6 MW, for the hybrid system [28, 36,41].

Parameter	Symbol	Value	Unit
Turbine power	P	3.6	MW
Turbine rotational speed (cut in/out)	u_{in}/u_{out}	5–13	rpm
Operational wind speed range	V	4–25	m/s
Rated wind speed	u_R	16.5	m/s
Mass of the nacelle (NA)	m_{NA}	125	tonnes
Hub height from mean sea level	H	87	m
The density of tower and TP-S355 Steel	ρ	7860	kg/m^3
Tower data			
Top diameter	D_t	3	m
Bottom diameter	D_b	5	m
Weight	m_t	255	tonnes
Tower height	L_T	68	m
Wall thickness	t_T	0.027	m
Rotor and blade data			
Turbine rotor diameter	D	107	m
Swept area	TSA	8992	m^2
Mass of rotor+hub	m_R	100	tonnes
Rotor overhang	b	4	m
Blade root diameter	B_{root}	4	m
Blade tip chord length	B_{tip}	1	m
Blade length	L	52	m

Table 7. General information of tidal turbine, Atlantic Resources AR 2000, for the hybrid system [28,36].

Parameter	Symbol	Value	Unit
Turbine Power	P	2	MW
Turbine rotational Speed (Cut in/out)	Ω	1–3.05	rpm
Operational tidal speed range	V	1–4.5	m/s
Turbine rotor diameter	D	20	m
Height from the seabed	Z_S	25	m
Rotor Swept area	TSA	314	m^2
Mass of two turbines	m	300	tonnes

There are five scenarios for an offshore foundation design exposed to wind and wave loads [25], summarized in Table 8.

Table 8. Load case scenarios [36].

Scenario	Name and description	Wind model	Wave model	Alignment
E-1	Normal operational conditions. Wind and wave action in the same direction (no misalignment).	NTM at u_R (U-1)	1-yr ESS (W-1)	Collinear
E-2	Extreme wave load scenario. Wind and wave action in the same direction (no misalignment).	ETM at u_R (U-2)	50-yr EWH (W-4)	Collinear
E-3	Extreme wind load scenario. Wind and wave action in the same direction (no misalignment).	EOG at u_R (U-3)	1-yr EWH (W-2)	Collinear
E-4	Cut-out wind speed and extreme operating gust scenario. Wind and wave action in the same direction (no misalignment).	EOG at u_{out} (U-4)	50-yr EWH (W-4)	Collinear
E-5	Wind and wave misalignment scenario. Same as E-2, except the wind and wave are misaligned at an angle of $\phi = 90°$. Due to low aerodynamic damping, the dynamic amplification is higher in the cross-wind direction.	ETM at u_R (U-2)	50-yr EWH (W-4)	Misaligned at $\phi = 90°$

In Table 8, the Normal Turbulence Model (NTM) relates to the normal working conditions of the turbine. The Extreme Turbulence model (ETM) is for extreme turbulence conditions. The Extreme Operating Gust (EOG) is the highest single occurrence wind load by a sudden change in the wind speed. ESS and EWH denote Extreme Sea State and Extreme Wave Height, respectively. The significant wave height Hs, used in ESS scenarios, is the average of the maximum one-third of all waves in the three hours, while the maximum wave height Hm, used in EWH scenarios, is the maximum wave height for three hours [36].

5. Results

5.1. Wind loads

In this section, the main parameters of the wind scenarios are calculated. The loads and moments will be used later in section 5.3 to identify driving combined scenarios, either E1 or E5.

Wind scenario U-1: Normal Turbulence (NTM) at Rated Wind Speed (U_R):

The mean wind speed is the rated wind speed (U_R) where the highest thrust force (Th) is expected, and the wind turbulence is modelled by the Normal Turbulence Model (NTM). This scenario is typical for the normal operation of the turbine. The standard deviation of wind speed in normal turbulence following IEC (2005) can be written as

$$\sigma_{u,NTM} = I_{ref}(0.75u + b) \quad \text{with} \quad b = 5.6\ m/s \tag{1}$$

where I_{ref} is the reference turbulence intensity (expected value at u = 15[m/s]), $\sigma_{u,NTM}$ is the standard deviation of wind speed in the normal turbulence model (NTM), and b is the model parameter defined as 5.6 according to IEC 2005. For the calculation of the maximum turbulent wind speed component (u_{NTM}), the time constant of the pitch control is assumed to be the same as the time period of the rotation of the rotor. In other words, it is assumed that the pitch control can follow changes in the wind speed that occur at a lower frequency than the turbine's rotational speed. Then maximum turbulent wind speed component (u_{NTM}) may be determined by calculating the contribution of variations in the wind speed with a higher frequency than f_{1P}, max to the total standard deviation of wind speed. From the Kaimal spectrum used for the wind turbulence process, its standard derivation can be calculated using Eq (2).

$$\sigma_{u,NTM,f>f_{1P}} = \sigma_{u,NTM}\sqrt{\frac{1}{(\frac{6L_k}{u_R}f_{1P,max}+1)^{\frac{2}{3}}}} \tag{2}$$

where $\sigma_{u,NTM,f>f_{1P}}$ is the variations in the wind speed with a higher frequency than f_{1P}, $\sigma_{u,NTM}$ is the standard deviation of wind speed in normal turbulence, L_k is the integral length scale, u_R is rated wind speed, and f_{1P} is the rotor's rotation frequency (1P).

The turbulent wind speed encountered in normal operation in normal turbulence conditions is found by assuming a normal distribution of the turbulent wind speed component and taking the 90% confidence level value. This is substituted into the quasi-static equation used in Eq (4). Equation (5) shows expressions for the corresponding wind moment at the mudline [36].

$$u_{NTM} = 1.28\sigma_{u,NTM,f>f_{1P}} \tag{3}$$

$$F_{wind,NTM} = \frac{1}{2}\rho_a A_R C_T (u_R + u_{NTM})^2 \tag{4}$$

$$M_{wind,NTM} = F_{wind,NTM}(S + z_{hub}) \tag{5}$$

where u_{NTM} is the maximum turbulent wind speed component, $\sigma_{u,NTM,f>f_{1P}}$ is the variations in the wind speed with a higher frequency than f_{1P}, ρ_a is the air density, A_R is rotor swept area, C_T is the thrust coefficient, u_R is rated wind speed, $F_{wind,NTM}$ and $M_{wind,NTM}$ are mudline load and moment in normal turbulence, S is water depth, and z_{hub} is hub height.

I_{ref} is assumed to be 16% from Table 4. Thus, $\sigma_{u,NTM} = 0.16(0.75 \times 15 + 5.6) = 2.69\, m/s$. 1.1 $f_{1P,\,max}$ is assumed to be 0.24 Hz or $f_{1P,\,max}$= 0.218 Hz from Table 5. L_K is assumed to be 340.2 m from Table 4 and u_R= 16.5 m/s from Table 6. So, $\sigma_{u,NTM,f>f_{1P}}$ (Eq (2)) will be 0.89 m/s. This value in Eq (3) results, $u_{NTM} = 1.28 \times 0.89 = 1.13\, m/s$. Using the total wind load and moment for the Terawhiti are estimated as $F_{wind,\,NTM}$ =1.68 [MN], $M_{wind,NTM}$ =374.64 [MNm]

Wind scenario U-2: Extreme Turbulence (ETM) at Rated Wind Speed (U_R):

The ETM calculates the standard deviation of wind speed at the rated wind speed and, from that, the maximum wind load under normal operation in extreme turbulence conditions. The standard deviation of wind speed in ETM is given in IEC (2005) as

$$\sigma_{u,ETM} = cI_{ref}\left[0.072\left(\frac{u_{avg}}{c}+3\right)\left(\frac{u_R}{c}-4\right)+10\right] \quad \text{with} \quad c = 2\ [m/s] \tag{6}$$

where Eq (6) terms are already defined (same as Eq (1)), but U_{avg} is the long-term average wind speed at the site. The maximum turbulent wind speed component u_{ETM} is determined similarly to the previous case.

$$\sigma_{u,ETM,f>f_{1P}} = \sigma_{u,ETM}\sqrt{\frac{1}{\left(\frac{6L_k}{u_R}f_{1P,max}+1\right)^{\frac{2}{3}}}} \tag{7}$$

The turbulent wind speed encountered in normal operation in extreme turbulence conditions, which is used for cyclic/dynamic load analysis, is found by assuming a normal distribution of the turbulent wind speed component. Unlike normal turbulence situations, the 95% confidence level value is taken. This is substituted into the quasi-static equation used in Eq (4). Equation (10) shows the expression for wind moments at the mudline [36].

$$u_{ETM} = 2\sigma_{u,ETM,f>f_{1P}} \tag{8}$$

$$F_{wind,ETM} = \frac{1}{2}\rho_a A_R C_T (u_R + u_{ETM})^2 \tag{9}$$

$$M_{wind,ETM} = F_{wind,ETM}(S + z_{hub}) \tag{10}$$

where Eqs (8) to (10) terms are already defined (same as Eqs (3) to (5)), but U_{avg} from Table 4 is 7.1 m/s for Terawhiti. So, the results are estimated as:

$$\sigma_{u,ETM} = 3.1\ m/s, \quad \sigma_{u,ETM,f>f_{1P}} = 1.01\ m/s, \quad u_{ETM} = 2.02\ m/s,$$
$$F_{wind,ETM} = 1.86\ MN, \quad M_{wind,ETM} = 414.78\ MNm$$

Wind scenario U-3: Extreme operating Gust (EOG) at Rated Wind Speed (UR):

The EOG is a sudden change in the wind speed, and if it hits the rotor when it is operating at the turbine's rated wind speed, the wind turbine's pitch control has no time to alleviate the loading. IEC (2005) suggests that for simplified foundation design, 50-year extreme operating gust (EOG) is assumed to estimate the highest single occurrence wind load. The 50-year extreme wind speed, which is typically used in wind turbine design for extreme wind conditions, can be determined by standard Eqs (11) to (14) sourced from Bhattacharya [36].

$$U_{10,50-year} = K[-\ln(1 - 0.98^{\frac{1}{52596}})]^{\frac{1}{s}} \quad (11)$$

where the number 52596 = 365.25[days/year] × 24[hours/day] × 6[10 min intervals/hour] represents the number of 10-minutes intervals in a year. The 10-year extreme wind speed is represented by

$$u_{10,1-year} = 0.8U_{10,50-year} \quad (12)$$

The characteristic standard deviation of wind speed can be calculated by

$$\sigma_{U,c} = 0.11U_{10,1-year} \quad (13)$$

which c is the return period of EOG.

The extreme gust speed is then calculated at the rated wind speed from

$$u_{EOG} = \min\left\{1.35\left(u_{10,1-year} - u_R\right); \frac{3.3\sigma_{u,c}}{1+\frac{0.1D}{\Lambda_1}}\right\} \quad (14)$$

where D is the rotor diameter = 107 m, $\Lambda_1 = L_k/8$, with L_k being the integral length scale. Using this, the total wind load is estimated as

$$F_{wind,EOG} = Th_{EOG} = \frac{1}{2}\rho_a A_R C_T (u_R + u_{EOG})^2 \quad (15)$$

where Eq (15) terms are already defined (same as Eqs (4)), for wind speeds between cut-in and cut-out, thrust coefficient is estimated as recommended by Arany et al. [42]:

$$C_T \approx \frac{7}{\bar{u}} \quad (16)$$

Using Eq (16), $C_T = 7/\bar{u} = 7/7.1 = 0.98$ and rated wind speed u_R= 16.5 m/s. Using the water depth S and the hub height above sea level z_{hub}, the mudline bending moment (without the load factor γ_L) can be estimated using Eq (17) sourced from [36].

$$M_{wind,\,EOG} = F_{wind,\,EOG}(S + z_{hub}) \quad (17)$$

The EOG wind speed is calculated using data from Table 5 and Eqs (11) to (14)

$$U_{10,50-year} = 31.1\ \text{m/s}, u_{10,1-year} = 24.8\ \text{m/s}, \sigma_{U,c} = 2.7\ \text{m/s},\ u_{EOG} = 7.1\ \text{m/s}$$

Using this, the total wind load is estimated as $F_{wind,\,EOG}$

$$Th_{wind,\,EOG} = \frac{1}{2} \times 1.225 \times \frac{\pi}{4}(107)^2 \times \frac{7}{7.1} \times (16.5 + 7.1)^2 \approx 3[\text{MN}]$$

and using the water depth S =110 [m] and the hub height above mean sea level z_{hub} = 103 [m]

$$M_{wind,\,EOG} = 3\,(110 + 103) = 639\ [\text{MNm}]$$

Wind scenario U-4: Extreme operating Gust (EOG) at the Cut-Out Wind Speed (U_{out}):

If the 50-year EOG hits the rotor slightly below the cut-out speed of the turbine due to the sudden

change in wind speed, the turbine cannot shut down. Note that the EOG calculated at the cut-out wind speed differs from that evaluated at the rated wind speed according to IEC 2005.

Wind load caused by the EOG at the cut-out wind speed U_{out} is calculated taking into consideration that according to thrust coefficient expression of Frohboese and Schmuck 2010 (Eq (16)) [43] is no longer valid. Instead, it should be determined by assuming that the pitch control keeps the power constant. This means that the thrust force is inversely proportional to the wind speed above the rated wind speed U_R and the thrust coefficient is inversely proportional to the cube of the wind speed. So, between cut-in (U_{in}) and rated wind speed (U_R), Eq (16) is used for calculating the thrust coefficient and after rated wind speed, Eq (18) is used for calculating the thrust coefficient.

$$C_T = \frac{7u_R^2}{u^3} \tag{18}$$

The EOG speed at cut-out wind speed $u_{EOG,Uout}$ is determined from Eqs (11) to (14) by substituting a value for U_{out} (which is not the same at U_R). The thrust force and moment can be estimated using Eqs (19) and (20) sourced from [36].

$$\mathrm{T_{wind,\,u}}_{out} = \frac{1}{2}\rho_a A_R C_{DT}(u_{out} + u_{EOG,u_{out}})^2 \tag{19}$$

$$\mathrm{M_{wind,\,u}}_{out} = (S + z_{hub})\,\mathrm{T_{wind,\,u}}_{out} \tag{20}$$

where Eqs (19) & (20) terms are already defined (same as Eqs (4) & (5)). So, using Eq (14) $u_{EOG,u_{out}} =$ 7.1 m/s and as a result:

$$\mathrm{T_{wind,\,u}}_{out} = \frac{1}{2} \times 1.225 \times \frac{\pi}{4}(107)^2 \times \frac{7\times16.5^2}{25^3} \times (25 + 7.1)^2 = 0.69\ [\mathrm{MN}]$$

$$\mathrm{M_{wind,\,EOG}} = 0.69\,(110 + 103) = 146.9\ [\mathrm{MNm}]$$

Table 9 summarizes the important parameters and presents the wind loads for the different wind scenarios to determine the turbulent wind speed component and, through that, the thrust force and overturning moment. The wind loads on the structure are independent of the substructure diameter; therefore, the wind loads can be evaluated before the pile and substructure design are available.

Table 9. Load and overturning moment of wind scenarios (U-1)–(U-4) for Terawhiti.

Parameters	Wind scenario (U-1)	Wind scenario (U-2)	Wind scenario (U-3)	Wind scenario (U-4)
The standard deviation of wind speed $\sigma_U[m/s]$	2.69	3.1	2.7	2.7
Standard deviation in $f > f_{1P}$	0.89	1.01	-	-
Turbulent wind speed component $u[m/s]$	1.13	2.02	7.1	7.1
Total wind load F_{wind} [MN]	1.68	1.86	3	0.69
Total wind moment M_{wind} [MNm]	374.64	414.78	639	146.9

Applying an environmental load factor of $\gamma_L = 1.35$ as recommended by DNV 2014 [26] and IEC 2019 [24], the total wind moment is 862.65 [MNm] for U3. It is found that the EOG at U_R (U-3) gives the highest load and overturning moment.

5.2. Wave loads

The wave conditions recommended by Bhattacharya [36] for calculating critical wave loads acting on the substructure are:

(W-1) One-year extreme sea state (ESS). A wave with height equal to the 1-year significant wave height $H_{S,1}$.

(W-2) One-year extreme wave height (EWH). A wave with a height equal to the 1-year maximum wave height $H_{m,1}$.

(W-3) 50-year ESS. A wave with a height equal to the 50-year significant wave height $H_{S,50}$.

(W-4) 50-year EWH. A wave with a height equal to the 50-year maximum wave height $H_{m,50}$.

Bhattacharya [36] states that the one-year ESS and EWH are used as a conservative overestimation of the normal wave height ($_{NWH}$) prescribed in IEC 2019 [24]. In relation to the ESS, it is important to note that the significant wave height and the maximum wave height have different meanings. The significant wave height H_S is the average of the highest one-third of all waves in the three-hour sea state, while the maximum wave height Hm is the single highest wave in the same three-hour sea state.

The highest wind load is expected to be caused by scenario U-3, and the highest wave load is due to scenario W-4. In practice, the 50-year extreme wind load and the 50-year extreme wave load have a negligible probability of occurring at the same time and the DNV.

2014 code [26] also doesn't require these extreme load cases to be evaluated together. The designer has to find the most severe event with a 50-year return period based on the joint probability of wind and wave loading. Therefore, for the ULS analysis, two combinations are suggested by Arany et al. 2017 [42]:

(1) The ETM wind load at rated wind speed combined with the 50-year EWH–the combination of wind scenario U-2 and wave scenario W-4. This will provide higher loads in deeper water with higher waves.

(2) The 50-year EOG wind load combined with the one-year maximum wave height.

This will provide higher loads in shallow water in sheltered locations where wind load dominates. These scenarios are somewhat more conservative than those required by standards and can be adapted for simplified analysis. From the point of view of SLS and FLS, the single largest loading on the foundation is not representative because the structure is expected to experience this level of loading only once throughout its lifetime.

In simplified load calculation methodologies, simple linear waves are assumed to determine the wave loading. Higher-order theories like Stokes waves or Dean's stream function theory would provide better estimates, especially in shallow waters. However, the linear theory allows for simpler load calculation, and its application is justified for foundation design loads.

The circular substructure area A_S is also calculated from this diameter. The methodology used here builds on linear (Airy) wave theory, which gives the surface elevation η, horizontal particle velocity w, and the horizontal particle acceleration $\dot{w}$ as

$$\eta(x,t) = \frac{H_m}{2}\cos\left(\frac{2\pi t}{T_S} - kx\right) \tag{21}$$

$$w(x,z,t) = \frac{\pi H_m \cosh(k(S+z))}{T_S \sinh(KS)}\cos\left(\frac{2\pi t}{T_S} - kx\right) \tag{22}$$

$$\dot{w}(x,z,t) = \frac{-2\pi^2 H_m \cosh(k(S+z))}{T_S^2 \sinh(kS)} \sin(\frac{2\pi t}{T_S} - kx) \tag{23}$$

where H_m is maximum wave height, T_s is peak wave period, S is mean water depth, t is time, and x is the horizontal coordinate in the along-wind direction. The wave number k is obtained from the dispersion relation

$$\omega^2 = gk\tanh(kS) \quad \text{with} \quad \omega = \frac{2\pi}{T_S} \tag{24}$$

The force on a unit length strip of the substructure is the sum of the drag force F_D and the inertia force F_I:

$$dF_{wave}(z,t) = dF_D(z,t) + dF_I(z,t) = \frac{1}{2}\rho_w D_S C_D w(z,t)|w(z,t)| + C_m \rho_w A_S \dot{w}(z,t) \tag{25}$$

where w horizontal particle velocity is a function of z coordinate and t time, the C_D is the drag coefficient, C_m is the inertia coefficient, ρ_w is the density of seawater, D_S and A_S are the diameter and circular substructure area. The total horizontal force and bending moment at the mudline are then given by integration as

$$F_{wave}(t) = \int_{-S}^{\eta} dF_D\, dz + \int_{-S}^{\eta} dF_I\, dz \tag{26}$$

$$M_{wave}(t) = \int_{-S}^{\eta} dF_D(S + z_{hub})\, dz + \int_{-S}^{\eta} dF_I(S + z_{hub})\, dz \tag{27}$$

The peak load of the drag and inertia loads occur at different time instants; therefore, the maxima are evaluated separately. The maximum inertia load occurs at the time instant t = 0 when $\eta = 0$, and the maximum of the drag load occurs when t = $T_S/4$ and $\eta = H_m/2$.
The maximum drag load & moment $F_{D,max}$ & $M_{D,max}$ is then obtained by carrying out the integrations:

$$F_{D,max} = \frac{1}{2}\rho_w D_S C_D \frac{\pi^2 H_m^2}{T_S^2 \sinh^2(kS)} P_D(k,S,\eta) \tag{28}$$

$$M_{D,max} = \frac{1}{2}\rho_w D_S C_D \frac{\pi^2 H_m^2}{T_S^2 \sinh(kS)} Q_D(k,S,\eta) \tag{29}$$

$$P_D(k,S,\eta) = \frac{e^{2k(S+\eta)} - e^{-2k(S+\eta)}}{8k} + \frac{S+\eta}{2} \tag{30}$$

$$Q_D(k,S,\eta) = (\frac{S+\eta}{8k} - \frac{1}{16k^2})e^{2k(S+\eta)} - (\frac{S+\eta}{8k} + \frac{1}{16k^2})e^{-2k(S+\eta)} + (\frac{S+\eta}{2})^2 + \frac{1}{8k^2} \tag{31}$$

The maximum inertia load & moment $F_{I,max}$ & $M_{I,max}$ are obtained by:

$$F_{I,max} = \frac{1}{2}\rho_w C_m D_S^2 \frac{\pi^3 H_m}{T_S^2 \sinh(kS)} P_I(k,S,\eta) \tag{32}$$

$$M_{I,max} = \frac{1}{2}\rho_w C_m D_S^2 \frac{\pi^3 H_m}{T_S^2 \sinh(kS)} Q_I(k,S,\eta) \tag{33}$$

$$P_I(k, S, \eta) = \frac{\sinh(k(S+\eta))}{k} \tag{34}$$

$$Q_I(k, S, \eta) = (\frac{S+\eta}{2k} - \frac{1}{2k^2})e^{k(S+\eta)} - (\frac{S+\eta}{2k} + \frac{1}{2k^2})e^{-k(S+\eta)} + \frac{1}{k^2} \tag{35}$$

In the simplified method for obtaining foundation loads, it can be conservatively assumed that the sum of the maxima of drag and inertia loads is the design wave load. This assumption is conservative because the drag and inertia load maxima occur at different time instants. All wave scenarios (W-1)–(W-4) are evaluated with the same procedure, using different values of wave height H and wave period T [36].

In this step, a simplified estimation of the extreme wave height and the corresponding wave period for a given site is explained, which involves the following sub-steps:

1. Obtain the relevant significant wave height H_S from a reliable source. The 1-year equivalents are calculated following DNV 2014 [26] from the 50-year significant wave height according to

$$H_{S,1} = 0.8H_{S,50} \tag{36}$$

Calculate the peak wave period corresponding to the significant wave height, T_S using:

$$T_S = 11.1\sqrt{\frac{H_S}{g}} \tag{37}$$

2. Calculate the number of waves in a 3-hour period, N: Typically, significant wave heights are given for a 3-hour period. In other words, this means that the significant wave height is calculated as the mean of the highest 1/3 of all waves. Therefore, many different wave heights occur within this 3-hour period, and the highest occurring wave height is called the maximum wave height H_m. To find this, one needs to know the number of waves in the 3-hour period because the more waves there are, the higher the chance of higher waves occurring.

$$N = \frac{3\text{hours}}{T_S} = \frac{10800\text{s}}{T_S} \tag{38}$$

3. Calculate the maximum wave height, H_m by

$$H_m = H_S\sqrt{\frac{1}{2}\ln(N)} \tag{39}$$

4. Calculate the peak wave period corresponding to the maximum wave height, Tm. The same formulae can be used as in step 2.

$$T_m = 11.1\sqrt{\frac{H_m}{g}} \tag{40}$$

The 50-year significant wave height, $H_{S,50}$ at Terawhiti can be found from NIWA [44]. ERA-40 Wave Atlas [35] provides an approximate value of 15 m shown in Table 11. So, according to Eq (36), $H_{S,1}$ is 12 m. Going to step 2, $T_{S,1}$ can be 12.2s. Equation (39) gives N = 885.24, and as a result, $H_{m,1}$ = 22.10 m and $T_{m,1}$= 16.66 s. Also, $H_{m,50}$ is 27.62m according to Eq (39). The wave periods for 4 scenarios are:

(W-1): $T_{S,1} = 11.1\sqrt{\frac{H_{S,1}}{g}} = 11.1\sqrt{\frac{12}{9.8}} = 12.2$ s

(W-2): $T_{m,1} = 11.1\sqrt{\frac{H_{m,1}}{g}} = 11.1\sqrt{\frac{22.10}{9.8}} = 16.66$ s

(W-3): $T_{S,50} = 11.1\sqrt{\frac{H_{S,50}}{g}} = 11.1\sqrt{\frac{15}{9.8}} = 13.73$ s

(W-4): $T_{m,50} = 11.1\sqrt{\frac{H_{m,50}}{g}} = 11.1\sqrt{\frac{27.62}{9.8}} = 18.63$ s

The wave heights and wave periods are summarized for all wave scenarios (W-1) to (W-4) in Table 10 according to the explanations presented.

Table 10. Wave heights and wave periods for different wave scenarios for Foveaux.

Parameters	Wave scenario (W-1)	Wave scenario (W-2)	Wave scenario (W-3)	Wave scenario (W-4)
Wave height H[m]	$H_{S,1}$=12	$H_{m,1}$=22.10	$H_{S,50}$=15	$H_{m,50}$=27.62
Wave period T[s]	$T_{S,1}$=12.2	$T_{m,1}$=16.66	$T_{S,50}$=13.73	$T_{m,50}$=18.63

The wave loads (Eqs (26) and (27)) are calculated only for the most severe wave scenarios used for Load Cases E-2 and E-3, i.e., wave scenario (W-2) and (W-4), the 1-year and 50-year extreme wave heights (EWHs), using the definitions presented in Table 8 where $\rho_w = 1030$ kg/m^3 and S = 110 m (from Table 2)

This section can be modelled using an equivalent diameter of D_D = 11.33 m for drag load calculations and D_I = 12.89 m for inertia load calculations.

C_D = 0.5 and C_m = 2 (based on DNV [26])

Hm, Ts, η, k for W-1 scenario: H_m = 12 m, T_s = 12.2 s, η = 0 for inertia loads and η = 6 m for drag loads, k = 0.034 m^{-1} (based on Eq (24))

Using Eqs (28) to (35) for the W-1 scenario:

$F_{D,max} = 0.57MN$, $M_{D,max} = 581.1$ MNm, $F_{I,max} = 0.37MN$, $M_{I,max} = 43.3\ MNm$

The results are:

$F_{wave,\ W\text{-}1} = 0.57 + 0.37 = 0.94$ MN, $M_{wave,\ W\text{-}1} = 581.1 + 43.3 = 624.4$ MNm

Hm, Ts, η, k for W-2 scenario: H_m = 22.10 m, T_s = 12.2 s, η = 0 for inertia loads and η = 11.05 m for drag loads, k=0.034m^{-1}(based on Eq (24))

Using Eqs (28) to (35) for the W-2 scenario:

$F_{D,max} = 2.8MN$, $M_{D,max} = 643.2\ MNm$, $F_{I,max} = 1.05MN$, $M_{I,max} = 86.7$ MNm

The results are:

$F_{wave,\ W\text{-}2} = 2.8+1.05 = 3.85$ MN, $M_{wave,\ W\text{-}2} = 643.2+86.7 = 729.9$ MNm

Hm, Ts, η, k for W-3 scenario: H_m = 15 m, T_s = 13.73 s, η = 0 for inertia loads and η = 7.5 m for drag loads, k = 0.029 m^{-1}(based on Eq (24))

Using Eqs (28) to (35) for the W-3 scenario:

$F_{D,max} = 0.93$ MN, $M_{D,max} = 13880.07$ MNM, $F_{I,max} = 0.24$ MN, $M_{I,max} = 1399.4$ MNm

The results are:

$F_{wave,\ W\text{-}3} = 1.2$ MN, $M_{wave,\ W\text{-}3} = 15279.4$ MNm

Hm, Ts, η, k for W-4 scenario: H_m = 27.62 m, T_s = 13.73 s, η = 0 for inertia loads and η = 13.81 m for drag loads, k = 0.029 m^{-1}(based on Eq (24))

Using Eqs (28) to (35) for the W-4 scenario:

$F_{D,max} = 0.04$ MN , $M_{D,max} = 5672.8\ MNM$, $F_{I,max} = 2.1\ MN$, $M_{I,max} = 1678.1\ MNm$

The results are:

$F_{wave,\ W\text{-}4} = 2.14$ MN, $M_{wave,\ W\text{-}4} = 7350.9$ MNm

5.3. Anchor load combinations for Ultimate Limit State (ULS)

The current load is calculated as [36]

$$F_C = \frac{1}{2}\rho_w D_D C_D V^2 B = \frac{1}{2} \times 1030 \times 11.33 \times 0.5 \times 1.32^2 \times 93 = 0.47 \quad (41)$$

The loads under the combined actions of wind and waves were calculated using different scenarios in Table 8 and adding the current load as below:

FE-1 = 1.68 + 0.94 + 0.47 = 3.09 MN

FE-2 = 1.86 + 2.14 + 0.47 = 4.47 MN

FE-3 = 3 + 3.85 + 0.47 = 7.32 MN

FE-4 = 0.69 + 2.14 + 0.47 = 3.3 MN

FE-5 = 1.86 + 2.14 + 0.47 = 4.47 MN

As expected, the wave load dominates, and the scenario with the combination of the 1-year EWH and the 50-year extreme operating gust (EOG) or E3 produces the ULS load. It should be noted here that this load is conservative for anchor design, as the load that acts on the anchor is reduced by the weight of the suspended section of the mooring line, the friction on the horizontal section (Touch Down Zone) of the mooring line, the soil reaction on the inverse catenary-shaped forerunner in the soil, and the weight of the forerunner. The vertical load acts on the spar at the instant when the surface elevation at the spar is at its highest point (wave crest). In contrast, the horizontal load is dominated by the inertia load, highest when the surface elevation is at the mean water level. Therefore, the ultimate load is taken as the horizontal load as calculated above [36].

5.4. Minimum caisson dimensions for Terawhiti with sandy soils

The diameter of the caisson D and the embedment depth L are the two main independent parameters that govern the holding capacity of the caisson for a given soil profile. Soil type is Soft/medium sand with the angle of internal friction of $\phi' = 30°$, effective unit weight of $\gamma' = 9$ and mooring chain friction on sand $\mu = 0.25$ [45].

The holding capacity of suction caissons is typically determined in terms of an envelope based on the horizontal and vertical load components at the anchor as:

$$FP = \left(\frac{H_u}{H_m}\right)^a + \left(\frac{V_u}{V_m}\right)^b \quad (42)$$

where

$$a = \frac{L}{D} + 0.5, \qquad b = \frac{L}{3D} + 4.5$$

H_m is the horizontal capacity, and V_m is the vertical capacity. On the other hand, H_u and V_u are the applied load. FP is the failure criterion, and the maximum value can be 1 (limiting condition). The horizontal capacity in the sand can be calculated as follows:

$$H_m = -LQ_{av} = 0.5A_bN_q\gamma'L^2 \tag{43}$$

where A_b is the effective unit bearing area of the forerunner (equals the diameter of the rope or wire, and 2.5–2.6 times the bar diameter for a chain), Nq is the bearing capacity factor as defined by:

$$N_q = e^{\pi\tan\phi}\tan^2(45° + \frac{\phi}{2}) \tag{44}$$

with ϕ being the internal angle of friction of the soil.

The vertical capacity in the sand will be

$$V_m = W' + \gamma' Z_e^2 y(\frac{h}{Z_e})(K\tan\delta)_e(\pi D_e) + \gamma' Z_i^2 y(\frac{h}{Z_i})(K\tan\delta)_i(\pi D_i) \tag{45}$$

where

$$Y(x) = e^{-x} - 1 + x$$

$K\ tan\delta$: the factor that only appears together.

K: the effective stress factor used to calculate the effective horizontal stress as constant times the effective vertical stress ($\sigma_H = K\sigma_V'$), δ is the mobilized angle of friction between the caisson wall and the soil, e represents the external, and i is the internal circumference of the caisson.

Z: D/[4K tan δ] with e and i referring to external and internal values, respectively.

The anchor padeye tensions and angles can be determined by (look at Figure 6):

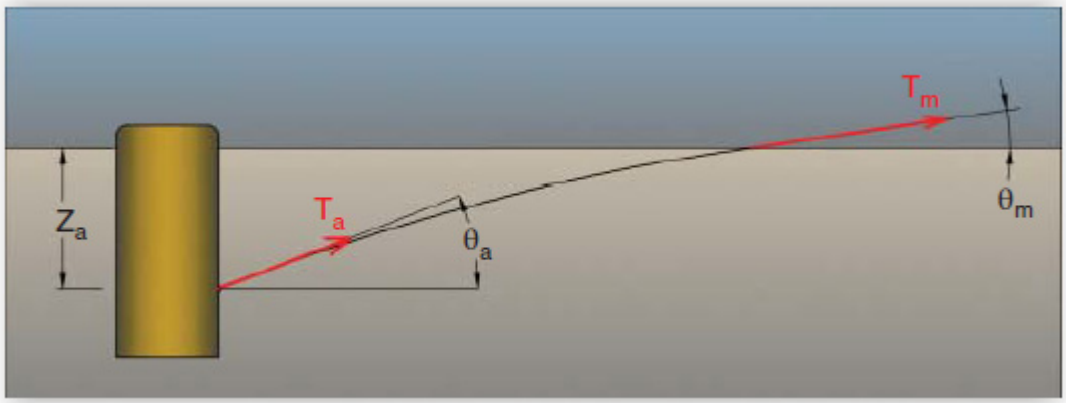

Figure 6. Loads on the anchor lines [36].

$$\frac{T_a}{2}(\theta_a^2 - \theta_m^2) = z_aQ_{av} \tag{46}$$

$$\frac{T_m}{T_a} = e^{\mu(\theta_a - \theta_m)} \tag{47}$$

where

T_a tension at the anchor padeye.

T_m tension at the mudline.

θ_a angle of the tension at the anchor padeye to horizontal.

θ_m angle of the tension at the mudline to horizontal.
z_a depth of the anchor padeye below mudline.
μ friction coefficient between the forerunner (chain, rope, or wire) and the soil.
Q_{av} average soil resistance between the mudline and the padeye is calculated as:

$$z_a Q_{av} = A_b N_c \int_0^{z_a} \gamma' z dz \quad (48)$$

where N_c is the bearing capacity factor and between 9 and 14, $s_u(z)$ is the distribution of the undrained shear strength with depth.

For sand, $z_a/L=2/3$ [36]. Statoil 2015 [27] advised each anchor's maximum diameter of 7 m. As this design is a hybrid design of Hywind statoil by adding tidal turbines and considering wind and tidal conditions of New Zealand, the caisson dimensions will be according to [13]:

Table 11. Caisson dimensions for the hybrid system.

Parameter	Symbol	Value
Length-to-diameter ratio	L/D	3.2
Caisson diameter [m]	D	6.9
Corresponding length [m]	L	22.07
Wall thickness [m]	t_w	0.099
The effective weight of caisson [kN]	W_c	3361
External skin friction factor [-]	$(K \tan\delta)_e$	7
Internal skin friction factor [-]	$(K \tan\delta)_i$	5
External shaft friction [kN]	F_e	7343
Internal shaft friction [kN]	F_i	6901
Maximum vertical load capacity [kN]	V_m	14247
Maximum horizontal load capacity [kN]	H_m	278358
Anchor padeye depth [m]	z_a	14.72
Padeye location [%]	r_z	0.67
Angle at the padeye [deg]	θ_a	50.14
Tension at the padeye (variable) [kN]	T_a	18561
Horizontal load on the anchor [kN]	H_u	11897
Vertical load on the anchor [kN]	V_u	14247
Horizontal load check exponent	a	3.7
Vertical load check exponent	b	5.5667
Vertical utilization	V_u/ V_m	1
Horizontal utilization	H_u/ H_m	0.04

6. Discussion and conclusions

The aim of this paper is to develop a unique method for structural design of hybrid offshore systems in deep waters using spar buoy floating. The method enables to find required dimensions tolerating against wind and wave loads. Terawhiti in Cook Strait was selected as a case study because according

to MetOcean model, this location can generate maximum electricity and suitable for this type of foundation. Based on the selection of turbines and Terawhiti as facility site and by including the wind and wave loads, the design provides the stability of structure.

The wind and water produce aerodynamic and hydrodynamic loads (thrust and drag) on the structure which depends on the operational speed of turbines. But, to know the acceptability of foundation design, it is necessary to combine wind and wave loads in ULS design and calculate maximum loads and find driven scenario. Based on different scenarios of foundation design, next step will be calculating maximum loads, and find driven scenario. Then, the minimum required sizes of caisson based on the maximum load of the driven scenario for the Hybrid floating offshore structure can be estimated. These dimensions satisfy the failure criterion.

The results, as presented and discussed in Section 5, enable several conclusions:

- The highest wind load for ULS is determined from the 50-year extreme operating gust (EOG); this is wind scenario U-3 which is 3 MN. Total wind loads for U-2, U-1 and U-4 are 1.86, 1.68 and 0.69 MN respectively.
- The maximum drag and inertia loads occurs for wave scenario (W-2) with the 1-year EWH which are 2.8 and 1.05 MN respectively or totally 3.85 MN. This values for W-1, W-3 and W-4 are 0.94, 1.2 and 2.14 MN respectively.
- The maximum load occurs in extreme wind load scenario when wind and wave act in same direction or E-3. This equals to combined values of U-3 and W-2 which is 7.32 MN. It is higher than combined wind and wave loads of scenarios E-1, E-2, E-4 and E-5 (as defined in Table 8) which are 3.09, 4.47, 3.3 and 4.47 MN respectively. Based on mentioned maximum load, the required diameter of the caisson and the embedment depth are 6.9 and 22.07 meter respectively.

The future work in this aspect can be estimating the cost analysis in terms of comparing the proposed hybrid system with a wind floating and with a floating tidal system and analyzing how much using the same structure for both wind, and tidal turbines can reduce the cost of electricity generation rather than having a foundation design just for wind and also just for tidal turbines.

Funding

This research did not receive any specific grant from public, commercial, or not-for-profit funding agencies.

Data availability statement

Data is available on request from the authors.

Conflicts of interest

The authors declare no conflict of interest.

References

1. Li L (2018) Dynamic response and power production of a floating integrated wind, wave and tidal energy system. *Renewable Energy* 116: 412–422. https://doi.org/10.1016/j.renene.2017.09.080
2. Noori M, Kucukvar M, Tatari O (2015) Economic input-output based sustainability analysis of onshore and offshore wind energy systems. *Int J Green Energy* 12: 939–948. https://doi.org/10.101080/15435075.2014.890103
3. Heptonstall P, Gross R, Greenacre P, et al. (2012) The cost of offshore wind: Understanding the past and projecting the future. *Energy Policy* 41: 815–821. https://doi.org/10.1016/j.enpol.2011.11.050
4. Majdi Nasab N, Raabiul Islam Md, Muttaqi K, et al. (2021) Optimization of a grid-connected microgrid using tidal and wind energy in Cook Strait. *Fluids* 6: 426. https://doi.org/10.3390/fluids6120426
5. Gruszczynski A, Hambrey D, Romero Jimenez E, et al. (2017) Hybrid offshore wind and tidal. Available from: http://www.esru.strath.ac.uk/EandE/Web_sites/16-17/WindAndTidal/index.html.
6. Zhao T, Xu M, Xiao X, et al. (2021) Recent progress in blue energy harvesting for powering distributed sensors in ocean. *Nano Energy* 88: 106199. https://doi.org/10.1016/j.nanoen.2021.106199
7. Sarma N, Tuohy PM, Mohammed A, et al. (2021) Rotor electrical fault detection in DFIGs using wide-band controller signals. *IEEE Trans Sustainable Energy* 12: 623–633. https://doi.org/10.1109/tste.2020.3014446
8. Karumalai D, Palanisamy AP, Palanisamy AK, et al. (2020) Offshore integrated renewable power system. In IOP Conference Series: *Mater Sci Eng* IOP Publishing. https://doi.org/10.1088/1757-899X/955/1/12074
9. Pérez-Collazo C, Greaves D, Iglesias G (2015) A review of combined wave and offshore wind energy. *Renewable Sustainable Energy Rev* 42: 141–153. https://doi.org/10.1016/j.rser.2014.09.032
10. Christensen ED, Stuiver M, Guanche R, et al. (2015) Go offshore-Combining food and energy production. Technical University of Denmark, Department of Mechanical Engineering.
11. H2OCEAN. Available from: http://www.vliz.be/projects/mermaidproject/project/related-projects/h2ocean.html.
12. Lin YH, Kao SH, Yang CH (2019) Investigation of hydrodynamic forces for floating offshore wind turbines on spar buoys and tension leg platforms with the mooring systems in waves. *Appl Sci* 9: 608. https://doi.org/10.3390/app9030608
13. Arany L, Bhattacharya S (2018) Simplified load estimation and sizing of suction anchors for spar buoy type floating offshore wind turbines. *Ocean Eng* 159: 348–357. https://doi.org/10.1016/j.oceaneng.2018.04.013
14. Mirzaei F, Tavakoli A, Tashakori Z (2018) Stability analysis of TLP floating wind turbine under severe environmental loading condition. Available from: http://hal.archives-ouvertes.fr/hal-01856187.
15. Chen C, Ma Y, Fan T (2022) Review of model experimental methods focusing on aerodynamic simulation of floating offshore wind turbines. *Renewable Sustainable Energy Rev* 157: 112036. https://doi.org/10.1016/j.rser.2021.112036
16. Farr H, Ruttenberg B, Walter RK, et al. (2021) Potential environmental effects of deepwater floating offshore wind energy facilities. *Ocean Coastal Manage* 207: 105611. https://doi.org/j.oceoaman.2021.105611

17. Ballast in spar buoy. Available from: https://www.theguardian.com/environment/2014/jun/23/drifting-off-the-coast-of-portugal-the-frontrunner-in-the-global-race-for-floating-windfarms.
18. Musial W, Butterfield S, Boone A (2004) Feasibility of floating platform systems for wind turbines. *In 42nd AIAA aerospace sciences meeting and exhibit*. https://doi.org/10.2514/6.2004-1007
19. Fontana CM, Arwade SR, Degroot DJ, et al. (2016) Efficient multiline anchor systems for floating offshore wind turbines. In International Conference on Offshore Mechanics and Arctic Engineering. *American Society of Mechanical Engineers*. https://doi.org/10.1115/OMAE2016-54476
20. Diaz BD, Rasulo M, Aubeny CP (2016) Multiline anchors for floating offshore wind towers. *In OCEANS 2016 MTS/IEEE Monterey. IEEE*. https://doi.org/10.1109/OCEANS.2016.7761374
21. Balakrishnan K, Arwade SR, Degroot DJ, et al. (2020) Comparison of multiline anchors for offshore wind turbines with spar and with semisubmersible. *J Physics: Conference Series*. IOP Publishing. https://doi.org/10.1088/1742-6596/1452/1/012032
22. Goldschmidt M, Muskulus M (2015) Coupled mooring systems for floating wind farms. *Energy Procedia* 80: 255–262. https://doi.org/10.1016/j.egypro.2015.11.429
23. IEC 61400. Available from: https://en.wikipedia.org/wiki/IEC_61400.
24. BS EN IEC 61400-3-1: 2019 (2019) Wind energy generation systems. Design requirements for fixed offshore wind turbines. 2019: BSI Standards Limited. Availabe from: https://standards.govt.nz/shop/bs-en-iec-61400-3-12019.
25. Bortolotti P, Tarres HC, Dykes K, et al. (2019) IEA Wind TCP Task 37: Systems engineering in wind energy-WP2.1 reference wind turbines. *National Renewable Energy Lab. (NREL)*, Golden, CO (United States). https://doi.org/10.2172/1529216
26. DNV G (2010) Environmental conditions and environmental loads. *Recommend Practice DNV-RP-C205.* Available from: https://home.hvl.no/ansatte/tct/FTP/H2021%20Marinteknisk%20Analyse/Regelverk%20og%20standarder/DnV_documents/RP-C205.pdf.
27. Statoil (2015) Hywind Scotland pilot park—Environmental statement. Available from: https://tethys.pnnl.gov/sites/default/files/publications/Hywind-Pilot-Park-Environmental-Statement.pdf.
28. Karimirad M (2014) Offshore energy structures: for wind power, wave energy and hybrid marine platforms. Springer. Available from: https://www.amazon.com/Offshore-Energy-Structures-Hybrid-Platforms/dp/331912174X.
29. Nasab NM, Kilby J, Bakhtiaryfard L (2021) Case Study of a hybrid wind and tidal turbines system with a microgrid for power supply to a remote off-grid community in New Zealand. *Energies* 14: 3636. https://doi.org/10.3390/en14123636
30. Limited D, Johnson D (2008) New Zealand's wave and tidal energy resources and their timetable for development. In International Conference on Ocean Energy (ICOE), Brest. Available from: https://www.semanticscholar.org/paper/New-Zealand-%E2%80%99-s-Wave-and-Tidal-Energy-Resources-and-Limited-Johnson/2a1bca8cc89688a4f8bdafeda4542e5129c0f6df.
31. Tidal Prediction Using TPX09, 2022. Available from: http://oceanomatics.com/.
32. Linz information about tides around New Zealand, 2006. Available from: https://www.linz.govt.nz/sea/tides/introduction-tides/tides-around-new-zealand.
33. Homer Pro (2020) Available from: https://www.homerenergy.com/.
34. NIWA Tide Forecaster (2020) Available from: https://tides.niwa.co.nz/.

35. The KNMI/ERA-40 Wave Atlas. (2020) Available from: http://projects.knmi.nl/wave_atlas/atlas_book.html#c57a.
36. Bhattacharya S (2019) Design of foundations for offshore wind turbines. John Wiley & Sons. Available from: https://www.wiley.com/en-us/Design+of+Foundations+for+Offshore+Wind+Turbines-p-9781119128120.
37. Weibull Calculator (2020) Available from: https://wind-data.ch/tools/weibull.php.
38. RETScreen (2018) Available from: https://www.nrcan.gc.ca/maps-tools-publications/tools/data-analysis-software-modelling/retscreen/7465.
39. Gupta R, Biswas A (2010) Wind data analysis of silchar (assam, India) by rayleighs and weibull methods. *J Mechanical Eng Res* 2: 010–024. Available from: https://academicjournals.org/journal/JMER/article-full-text-pdf/9428F113700.
40. Ayodele TR, Jimoh AA, Munda JL, et al. (2012) Statistical analysis of wind speed and wind power potential of Port Elizabeth using Weibull parameters. *J Energy Southern Africa* 23: 30–38. https://doi.org/10.17159/2413-3051/2012/v23i2a3160
41. OPTUM CE (2010) Available from: https://optumce.com/.
42. Arany L, Bhattacharya S, Macdonald J, et al. (2017) Design of monopiles for offshore wind turbines in 10 steps. *Soil Dynamics Earthquake Eng* 92: 126–152. https://doi.org/10.1016/j.soildyn.2016.09.24
43. Frohboese P, Schmuck C, Hassan GG (2010) Thrust coefficients used for estimation of wake effects for fatigue load calculation. *In European Wind Energy Conference.* Available from: https://www.semanticscholar.org/paper/THRUST-COEFFICIENTS-USED-FOR-ESTIMATION-OF-WAKE-FOR-Frohboese-Hassan/6f1fdaec4f05daeb839c52e11109e403cf645e0a.
44. Taihoro Nukurangi (2007) Wave climate around New Zealand. NIWA. Available from: https://niwa.co.nz/our-science/coasts/research-projects/all/physical-hazards-affecting-coastal-margins-and-the-continental-shelf/news/waves#climate.
45. Crest Energy, 2019. Available from: http://www.crestenergyservices.com.